Mixed RIS-Relay NOMA-Based RF-UOWC Systems

Mohamed Elsayed[1], Ahmed Samir[1], Ahmad A.Aziz El-Banna[1], Wali Ullah Khan[2], Symeon Chatzinotas[2], Basem M. ElHalawany[1,*]
[1]Electrical Engineering Department, Faculty of Engineering at Shoubra, Benha University, Egypt
[2]Interdisciplinary Centre for Security, Reliability and Trust, University of Luxembourg, Luxembourg
[*]Corresponding Author
Emails: mohamed.elsayed@feng.bu.edu.eg, ahmed.saied@feng.bu.edu.eg, waliullah.khan@uni.lu, Symeon.Chatzinotas@uni.lu, basem.mamdoh@feng.bu.edu.eg

***Abstract*—Reconfigurable intelligent surface (RIS), non-orthogonal multiple access (NOMA), and underwater optical wireless communication (UOWC) are paradigms of technologies that drive the development of next generation communication systems. In this paper, we investigate the performance of a NOMA-based RIS-assisted hybrid radio frequency (RF)-UOWC system. The ship works as a relay that redirects the received signal to two underwater destinations simultaneously. Due to the interruption of the direct link between the base station and the ship floating on the surface of the water, communication will be carried out via an RIS fixed to an intermediate building. In this paper, we provide new analytical expressions for the outage probability (OP), asymptotic analyses of the OP, and diversity order (D) to gain insights into the system performance. The results showed that the diversity order depends on the UOWC receiver detection technique. In the end, we illustrated that the NOMA-based RIS-assisted system significantly improves the outage performance of hybrid RF-UWOC systems over a benchmark system.**

***Index Terms*—UWOC, Reconfigurable intelligent surfaces, Exponential-Generalized Gamma, decode and forward, non-orthogonal multiple access, outage probability.**

I. Introduction

Reconfigurable intelligent surface (RIS) is a promising efficient paradigm for many energy and spectral problems of the beyond fifth-generation (B5G) by adding programming capabilities over wireless channels [1]. Such a system is controlled via an intelligent microcontroller to guide the performance of the system in terms of scattering and reflection of the incident radio signals to achieve system requirements [2]–[4]. A resource allocation scheme was proposed to maximize the sum throughput of a RIS-assisted system was presented in [5]. The performance of RIS-based systems was proposed in many works [6]–[8], in [6] the authors studied the capacity of RIS-assisted multiple-input multiple-output (MIMO) symbiotic communications, while authors in [7] performed a comparison of RISs and amplify-and-forward relaying systems. In addition, the secrecy analysis of RIS-based wireless systems was analyzed in [9], [10].

Non-orthogonal multiple access (NOMA) has been recognized as a bright solution for many 5G and 6G applications including underwater internet of things (UIoT) and massive connection networks on account that it can improve the band and spectral efficiency [11]–[14]. Power domain NOMA (PD-NOMA) is the most common NOMA type in which the transmission is accomplished by superimposing different users' signals at different power levels, while a successive interference cancellation (SIC) is performed at the receiver to detect its own message [15]–[18].

The needs of underwater [19]–[21] and wireless communication have drawn a lot of attention to mixed underwater-RF networks, which have crucial application scenarios. In recent times, there has been a surge of interest in discovering the underwater ecosystem for a wide range of purposes, including oceanic animal research, oil rig monitoring, surveillance, and autonomous operations. Consequently, the hybrid RF-underwater optical wireless communication (UOWC) system has gotten a lot of attention, where different relaying protocols could be used such as amplify-and-forward, and decode-and-forward [22], [23]. The performance of RF-UOWC systems was proposed in many works [24]–[27]. The authors in [24], [25] investigate the outage probability (OP), average bit error rate (ABER), and ergodic capacity (EC) performance of a hybrid RF-UOWC system under different underwater turbulence scenarios. On another perspective, the secrecy performance of the hybrid RF-UOWC system was studied in the presence of an eavesdropper trying to intercept RF communications by the authors in [26], [27].

Although there is extensive research in the hybrid combination between RF and UOWC, to the best of our knowledge, only [28] investigated the effect of adding an RIS unit to a dual-hop hybrid RF-UOWC system in terms of OP and BER. However, the application of NOMA in RIS-assisted dual-hop mixed RF-UWOC communication systems has not been studied yet. Based on this incentive, we will conduct a study on a NOMA-based RIS-assisted dual-hop hybrid RF-UOWC system that suffers from an interruption in the direct link between the base station and a relay fixed on a ship floating on the surface of the water, so the communication will be carried out via an RIS mounted on a building. The main contributions of this paper can be summarized as follows: (1) Derive new closed-form and asymptotic expressions for the OPs of a downlink NOMA-based RIS-assisted hybrid RF-UWOC system assuming that the wireless channels are characterized by Rayleigh fading with an additive white Gaussian noise (AWGN) and the UOWC links are characterized by EGG

fading with AWGN. (2) Analyze the diversity order of the OPs. (3) Validate the analytical derivations through Monte-Carlo simulations for varying underwater scenarios of air bubbles level (BL) under thermally uniform and temperature gradient UOWC channels, then we analyze the impact of system parameters on the system performance. (4) Finally, we carried out a comparison between the proposed system with an orthogonal multiple access (OMA)-based benchmark system.

The rest of the paper is organized as follows, the system model is introduced in Section II. The performance of the considered system is analytically evaluated by deriving the OPs in Section III. Analytical and simulation results are discussed and compared with a benchmark system in Section IV. Finally, the conclusions are provided in Section V.

II. System Model

In this paper, we propose a downlink NOMA-based RIS-assisted hybrid RF-UWOC system shown in Fig.1, that combines base station (B), RIS, decode and forward relay (R) and two destinations D_i where $i \in \{1, 2\}$. The base station has an RF interface, and it needs to communicate with a far destination D_1 and a near destination D_2, both of which have an UWOC interface, the communication is carried out through an intermediate R that poses both RF and UOWC interfaces. Due to the long-distance and the obstacles, the direct link between B and R is broken, so the communication is achieved via N-elements RIS. This system is useful in many UIoT applications [29] such as offshore oil field exploration, oceanic monitoring, and data collection. The B-RIS and RIS-R channels (h_n and g_n) respectively are assumed to be characterized by Rayleigh fading with a mean of $\sqrt{\pi}/2$ under AWGN. The RF fading channels can be expressed as $h_n = \alpha_n e^{j\theta_n}$ and $g_n = \beta_n e^{j\psi_n}$ where $n \in \{1, 2, .., N\}$, α_n and θ_n are the channel amplitude and phase of h_n, respectively, while β_n and ψ_n are the channel amplitude and phase of g_n, respectively. The R-D_i channels (h_{D_i}) are characterized by EGG fading under AWGN.

To enhance the spectrum efficiency, we assume that B and R adopt PD-NOMA for multiplexing their messages. The communication is initiated, at B, by broadcasting a superimposed message $x_B = \sqrt{a_1 P_B} s_1 + \sqrt{a_2 P_B} s_2$ over RF channel, where s_1 and s_2 are the messages intended for D_1 and D_2 respectively, P_B is the total transmitted power at B, a_i is the NOMA power allocation factor of the signal intended for D_i. Without losing generality, we assume that $a_1 > a_2$ and $a_1 + a_2 = 1$. The received message at R through the RIS elements can be expressed as

$$y_R = \sum_{n=1}^{N} h_n \; r_n \; g_n \; x_B + n_\omega, \tag{1}$$

where n_ω represents AWGN with $n_\omega \sim \mathcal{CN}(0, \; \sigma_\omega^2)$ and $r_n = |r_n| \, e^{j\varphi_n}$ is reflection coefficient of the n-th RIS element. Additionally, we assume that all magnitudes $|r_n| = \alpha_n = \beta_n = 1$, while φ_n is the n-th RIS element adjustable phases and $\varphi_n = -(\theta_n + \psi_n)$. Accordingly, we can write $y_R = A(\sqrt{a_1 P_B} s_1 + \sqrt{a_2 P_B} s_2) + n_\omega$, where $A = \sum_{n=1}^{N} \alpha_n \beta_n$.

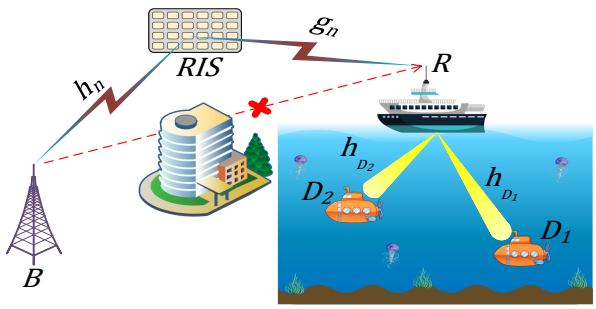

Figure 1. Downlink NOMA-based hybrid RF-UWOC system model

Using NOMA principle, R decodes s_1 firstly, and then applies the SIC operation, which is assumed to be imperfect, to decode s_2 . So, the signal-to-interference-plus noise ratios (SINRs) for decoding s_1 and s_2 are expressed as

$$\gamma_R^1 = \frac{a_1 \; \rho_B \; A^2}{a_2 \; \rho_B \; A^2 + 1}, \tag{2}$$

$$\gamma_R^2 = \frac{a_2 \; \rho_B \; A^2}{a_1 \; \rho_B \; \eta \; A^2 + 1}, \tag{3}$$

respectively, where $\rho_B = P_B/\sigma_\omega^2$, and $0 \leq \eta \leq 1$ is the residual power factor due to the imperfection of SIC operation. In the next step, R re-multiplexes the messages using PD-NOMA again and send them over the UWOC channels where each link is characterized by mixture EGG distribution [30]. The R transmitted message is $x_R = \sqrt{b_1 P_R} s_1 + \sqrt{b_2 P_R} s_2$ where P_R is the overall transmission power at R, b_i is the NOMA power allocation factor for D_i at R. Without loss of generality, $b_1 > b_2$ and $b_1 + b_2 = 1$. The received signal at the far destination through h_{D_1} link is $y_{D_1} = \zeta |h_{D_1}|^2 x_R + n_u$, where h_{D_1} is the EEG fading of UWOC link between R and D_1 with expectation $E[|h_{D_1}|^2] = 1$, ζ is responsivity which is considered to be unity and n_u is the AWGN with $n_u \sim \mathcal{CN}(0, \; \sigma_u^2)$. Consequently, D_1 decodes its message s_1 where the SINR for decoding s_1 at D_1 is

$$\gamma_{D_1}^1 = \frac{b_1 \; \rho_R \; |h_{D_1}|^2}{b_2 \; \rho_R \; |h_{D_1}|^2 + 1}, \tag{4}$$

where $\rho_R = P_R/\sigma_u^2$. Similarly the received signal at D_2 via h_{D_2} is $y_{D_2} = \zeta |h_{D_2}|^2 x_R + n_u$ where h_{D_2} is the EEG fading between R and D_2 with expectation $E[|h_{D_2}|^2] = 1$. D_2 follows the SIC principle to decodes s_1 before decoding its own message s_2. Thus, the SINRs for detecting s_1 and s_2 are

$$\gamma_{D_2}^1 = \frac{b_1 \; \rho_R \; |h_{D_2}|^2}{b_2 \; \rho_R \; |h_{D_2}|^2 + 1}, \tag{5}$$

$$\gamma_{D_2}^2 = \frac{b_2 \; \rho_R \; |h_{D_2}|^2}{b_1 \; \rho_R \; \eta |h_{D_2}|^2 + 1}, \tag{6}$$

respectively.

Channels Distributions: We characterize the UOWC channels h_{D_1}, h_{D_2} by the EGG distribution presented in [30], which take air bubbles level (BL) and temperature gradient (TG) into consideration to describe the underwater turbulence fading. EGG is a weighted mixture of both Exponential and Generalized Gamma distributions, it fits the practical results for different scenarios of channel

impairments of UWOC effectively. A closed-form expression for the cumulative distribution function (CDF) of EGG distribution is [30]

$$F_{|h_{D_i}|^2}(x)=wG_{1,2}^{1,1}\left(\frac{1}{\lambda}(\frac{x}{\mu_{r_1}})^{\frac{1}{r}}\middle|\begin{matrix}1\\1,0\end{matrix}\right)+\frac{1-w}{\Gamma(a)}G_{1,2}^{1,1}\left(\frac{1}{b^c}(\frac{x}{\mu_{r_1}})^{\frac{c}{r}}\middle|\begin{matrix}1\\a,0\end{matrix}\right), \tag{7}$$

where $0 < w < 1$ is the combination ratio between exponential and generalized gamma distribution, λ represents the exponential distribution scale parameter, (a, b, c) are the parameters of generalized gamma distribution, $G_{m,n}^{p,q}(.)$ is the Mejier-G function [31]. Based on the optical receiver technology, the average electrical SNR μ_{r_i} is determined. For heterodyne receiver $(r = 1)$, $\mu_{r_i} = \Omega_{x_i}$, while for intensity modulation/direct detection (IM/DD) $(r = 2)$, $\mu_{r_i} = \frac{\Omega_{x_i}}{2w\lambda^2+b^2(1-w)\Gamma(a+\frac{2}{c})/\Gamma(a)}$, where Ω_{x_i} is the average SNR. The values of EGG distribution parameters under different turbulence scenarios are practically determined in [30, Table I, II].

Since A is the sum of the product of two independent and identical Rayleigh distributed random variables (RVs), Based on [32, eq. 8] we can write its CDF as

$$F_A(x) = \frac{\gamma(1+\varepsilon, \frac{x}{v})}{\Gamma(1+\varepsilon)}, \tag{8}$$

where $\gamma(.,.)$ is the lower incomplete Gamma function [33, eq. 8.350.1], $\Gamma(.)$ is the Gamma function [33, eq. 8.310.1], $\varepsilon = \frac{k_1^2}{k_2} - 1$, $v = \frac{k_2}{k_1}$, $k_1 = \frac{N\pi}{2}$, and $k_2 = 4N(1 - \frac{\pi^2}{16})$.

III. OUTAGE PROBABILITY ANALYSIS

Now, to measure the system's performance, we derive closed-form expressions for the users' outage probabilities and the total system outage probability. To gain more insights into the system performance, the asymptotic outage probabilities and the diversity order for the proposed system are analyzed.

A. *Outage Probability* OP_1

The outage OP_1 occurs if R or D_1 fails to decode s_1, that can be written as

$$\begin{aligned} OP_1 &= 1 - \Pr(\gamma_R^1 > \gamma_1, \gamma_{D_1}^1 > \gamma_1) \\ &= 1 - \Pr(\frac{a_1\rho_B A^2}{a_2\rho_B A^2 + 1} > \gamma_1, \frac{b_1\rho_R|h_{D_1}|^2}{b_2\rho_R|h_{D_1}|^2 + 1} > \gamma_1) \\ &\overset{(a)}{=} 1 - \underbrace{\Pr(A > \sqrt{\frac{\tau_1}{\rho_B}})}_{P_0} \times \underbrace{\Pr(|h_{D_1}|^2 > \frac{\delta_1}{\rho_R})}_{P_1}, \end{aligned} \tag{9}$$

where (a) stems from the independence between A and h_{D_1}, $\gamma_1 = 2^{R_1} - 1$ and R_1 is the target data rate of s_1, $\tau_1 = \gamma_1/(a_1 - a_2\gamma_1)$ with $a_1 > a_2\gamma_1$ or $a_1 > \gamma_1/(1 + \gamma_1)$. Similarly, $\delta_1 = \gamma_1/(b_1 - b_2\gamma_1)$ with $b_1 > b_2\gamma_1$ or $b_1 > \gamma_1/(1 + \gamma_1)$. Using CDFs in (7), (8), we get

$$P_0 = 1 - \frac{\gamma(1+\varepsilon, \frac{\sqrt{\tau_1/\rho_B}}{v})}{\Gamma(1+\varepsilon)}, \tag{10}$$

$$P_1=1-wG_{1,2}^{1,1}\left(\frac{1}{\lambda}(\frac{\delta_1}{\rho_R\mu_{r_1}})^{\frac{1}{r}}\middle|\begin{matrix}1\\1,0\end{matrix}\right)-\frac{1-w}{\Gamma(a)}G_{1,2}^{1,1}\left(\frac{1}{b^c}(\frac{\delta_1}{\rho_R\mu_{r_1}})^{\frac{c}{r}}\middle|\begin{matrix}1\\a,0\end{matrix}\right). \tag{11}$$

B. *Outage Probability* OP_2

The outage OP_2 occurs if R or D_2 fails to decode s_1 or s_2, according to NOMA SIC principle that requires firstly decoding the strong message s_1 and then subtract it from received message before decoding s_2. Thus, OP_2 can be written as

$$\begin{aligned} OP_2 &= 1 - \Pr(\gamma_R^1 > \gamma_1, \gamma_R^2 > \gamma_2, \gamma_{D_2}^1 > \gamma_1, \gamma_{D_2}^2 > \gamma_2) \\ &= 1 - \left[\Pr(A^2 > \frac{\tau_1}{\rho_B}, A^2 > \frac{\tau_2}{\rho_B}, |h_{D_2}|^2 > \frac{\delta_1}{\rho_R}, |h_{D_2}|^2 > \frac{\delta_2}{\rho_R})\right] \\ &\overset{(b)}{=} 1 - \underbrace{\Pr(A > \sqrt{\frac{\tau}{\rho_B}})}_{P_2} \times \underbrace{\Pr(|h_{D_2}|^2 > \frac{\delta}{\rho_R})}_{P_3}, \end{aligned} \tag{12}$$

where (b) stems from the independence between A and h_{D_2}, $\gamma_2 = 2^{R_2} - 1$ and R_2 is the target data rate of s_2, $\tau_2 = \gamma_2/(a_2 - a_1\eta\gamma_2)$ with $a_2 > a_1\eta\gamma_2$ or $a_1 < 1/(1 + \eta\gamma_2)$. Similarly $\delta_2 = \gamma_2/(b_2 - b_1\eta\gamma_2)$ with $b_2 > b_1\eta\gamma_2$ or $b_1 < 1/(1 + \eta\gamma_2)$, $\tau = \max(\tau_1, \tau_2)$ and $\delta = \max(\delta_1, \delta_2)$. With the aid of CDFs in (7), (8), we can write

$$P_2 = 1 - \frac{\gamma(1+\varepsilon, \frac{\sqrt{\tau/\rho_B}}{v})}{\Gamma(1+\varepsilon)}, \tag{13}$$

$$P_3=1-wG_{1,2}^{1,1}\left(\frac{1}{\lambda}(\frac{\delta}{\rho_R\mu_{r_2}})^{\frac{1}{r}}\middle|\begin{matrix}1\\1,0\end{matrix}\right)-\frac{1-w}{\Gamma(a)}G_{1,2}^{1,1}\left(\frac{1}{b^c}(\frac{\delta}{\rho_R\mu_{r_2}})^{\frac{c}{r}}\middle|\begin{matrix}1\\a,0\end{matrix}\right). \tag{14}$$

C. *System Outage Probability* OP_{sys}

The total system outage OP_{sys} occurs if R or D_2 fails to decode any of the two messages or D_1 fails to decode s_1. It can be formulated as

$$\begin{aligned} OP_{sys} &= 1 - \Pr(\gamma_R^1 > \gamma_1, \gamma_R^2 > \gamma_2, \gamma_{D_2}^1 > \gamma_1, \gamma_{D_2}^2 > \gamma_2, \gamma_{D_1}^1 > \gamma_1) \\ &= 1 - \Pr(A^2 > \frac{\tau_1}{\rho_B}, A^2 > \frac{\tau_2}{\rho_B}, |h_{D_2}|^2 > \frac{\delta_1}{\rho_R}, \\ &\qquad |h_{D_2}|^2 > \frac{\delta_2}{\rho_R}, |h_{D_1}|^2 > \frac{\delta_1}{\rho_R}) \\ &\overset{(c)}{=} 1 - \underbrace{\Pr(A > \sqrt{\frac{\tau}{\rho_B}})}_{P_2}\underbrace{\Pr(|h_{D_2}|^2 > \frac{\delta}{\rho_R})}_{P_3}\underbrace{\Pr(|h_{D_1}|^2 > \frac{\delta_1}{\rho_R})}_{P_1}, \end{aligned} \tag{15}$$

where (c) stems from the independence between A, h_{D_1} and h_{D_2}. With the aid of (11), (13) and (14), we can obtain a closed form expression of OP_{sys} as in (16) at the top of the next page.

D. *Asymptotic Outage Probability*

To gain more insight about the system's performance, we derive the asymptotic outage probabilities under high SNRs scenario such that

$$\begin{aligned} OP_1^\infty &\approx 1 - P_0^\infty P_1^\infty, \\ OP_2^\infty &\approx 1 - P_2^\infty P_3^\infty, \\ OP_{sys}^\infty &\approx 1 - P_1^\infty P_2^\infty P_3^\infty, \end{aligned} \tag{17}$$

where P_z^∞ is the asymptotic of P_z and $z \in \{0, 1, 2, 3\}$. The asymptotic expression for P_0 and P_2 in obtained by substituting $\rho_B \to \infty$ in both (10) and (13) which leads to [33, eq. 8.350.5]

$$P_0^\infty = P_2^\infty \approx 1 - \frac{\gamma(1+\varepsilon, 0)}{\Gamma(1+\varepsilon)} \approx 1 - \frac{0}{\Gamma(1+\varepsilon)} \approx 1. \tag{18}$$

$$OP_{sys} = 1 - \left(1 - \frac{\gamma(1+\varepsilon, \frac{\sqrt{\tau/\rho_B}}{v})}{\Gamma(1+\varepsilon)}\right)\left(1 - wG_{1,2}^{1,1}\left(\frac{1}{\lambda}\left(\frac{\delta_1}{\rho_R\mu_r}\right)^{\frac{1}{r}}\middle|\begin{matrix}1\\1,0\end{matrix}\right) - \frac{1-w}{\Gamma(a)}G_{1,2}^{1,1}\left(\frac{1}{b^c}\left(\frac{\delta_1}{\rho_R\mu_r}\right)^{\frac{c}{r}}\middle|\begin{matrix}1\\a,0\end{matrix}\right)\right)$$
$$\times\left(1 - wG_{1,2}^{1,1}\left(\frac{1}{\lambda}\left(\frac{\delta}{\rho_R\mu_r}\right)^{\frac{1}{r}}\middle|\begin{matrix}1\\1,0\end{matrix}\right) - \frac{1-w}{\Gamma(a)}G_{1,2}^{1,1}\left(\frac{1}{b^c}\left(\frac{\delta}{\rho_R\mu_r}\right)^{\frac{c}{r}}\middle|\begin{matrix}1\\a,0\end{matrix}\right)\right). \quad (16)$$

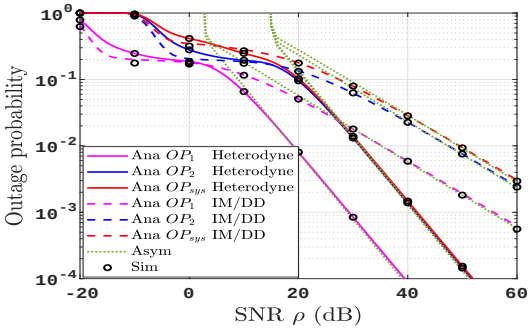

Figure 2. OPs versus SNR ρ for both IM/DD and heterodyne detection.

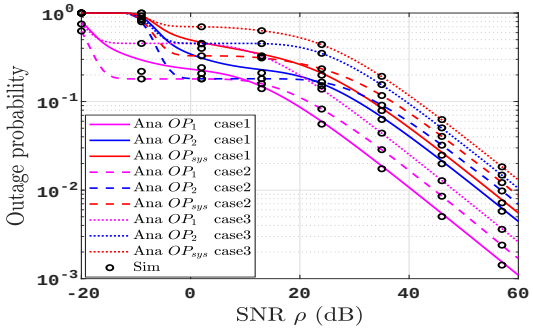

Figure 3. The effect of TG and BL on OPs performance.

Also a tight approximated expression for the CDF of the EGG distribution at high SNR is [30]

$$F_{|h_{D_i}|^2}(x) \simeq \frac{w}{\lambda}\left(\frac{x}{\mu_{r_i}}\right)^{\frac{1}{r}} + \frac{1-w}{\Gamma(a+1)}\left(\frac{x}{b^r\mu_{r_i}}\right)^{\frac{ac}{r}}, \quad (19)$$

Based on (19), we can obtain an asymptotic expressions for P_1 and P_3 as follows

$$P_1^{\infty} \approx 1 - \frac{w}{\lambda}\left(\frac{\delta_1}{\rho_R\mu_{r_1}}\right)^{\frac{1}{r}} - \frac{1-w}{\Gamma(a+1)}\left(\frac{\delta_1}{b^r\rho_R\mu_{r_1}}\right)^{\frac{ac}{r}},$$
$$P_3^{\infty} \approx 1 - \frac{w}{\lambda}\left(\frac{\delta}{\rho_R\mu_{r_2}}\right)^{\frac{1}{r}} - \frac{1-w}{\Gamma(a+1)}\left(\frac{\delta}{b^r\rho_R\mu_{r_2}}\right)^{\frac{ac}{r}}. \quad (20)$$

E. *Diversity Order*

In this section, we drive the outage diversity order (D) which is defined as the slope of outage curves at high SNR. According to [34], we can calculate diversity order as $D_l = -\lim_{\rho\to\infty}(\log(OP_l)/\log(\rho))$, where $l \in \{1, 2, sys\}$. According to (17), (18) and (20), we can write

$$D_l = \min\left(\frac{1}{r}, \frac{ac}{r}\right) \overset{d}{=} \frac{1}{r}, \quad (21)$$

where (d) stems from the fact that $\frac{ac}{r} >> \frac{1}{r}$ in all UOWC turbulence scenarios. This result is consistent with the plots in Fig.2.

IV. RESULTS AND DISCUSSIONS

In the following, we will discuss the outage performance of the proposed system by studying the effects of various system parameters that affect the quality and efficiency of the system. We justify our analytical results through an extensive Monte-Carlo simulation. The EGG UOWC parameters are set according to [30, Table I, II]. Unless otherwise specified in another context, we set the system parameters to a thermally uniform UOWC with 2.4 L/min bubble level with $\Omega_{x_1} = \Omega_{x_2} = 1$, $a_1 = b_1 = 0.7$, $\eta = 0.1$, $R_1 = 0.5$ bits/sec/Hz, $R_2 = 0.75$ bits/sec/Hz, and $\rho_B = \rho_R = \rho$. We denote "Ana, Asym, Sim" as symbols for analytical, asymptotic and Monte-Carlo simulation results, respectively.

Figure 2 presents the outage probability of the proposed system under the utilization of two different receiving technologies (heterodyne or IM/DD) with the same system parameters setting. The figure shows the superiority in favor of the heterodyne receiver as expected, but this will be at the expense of the complex design of the receiver. Also, we notice the perfect match between the analytical and simulation results over the entire range of SNR, besides the coincide between analytical and asymptotic results at high SNR, which validates the obtained formulas. According to (21), we expect a diversity order of 1 and 0.5 for heterodyne and IM/DD receivers, respectively, which agrees with the results in Fig. 2.

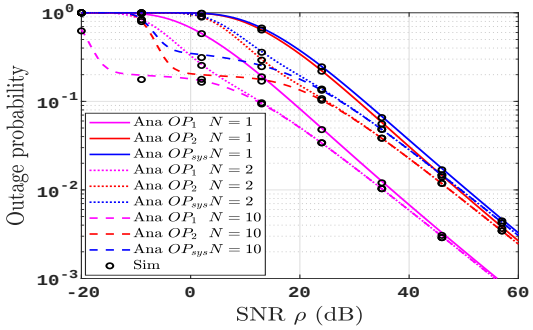

Figure 4. Effect of RIS number of elements on OPs performance.

Fig. 3 illustrates the effect of water turbulence parameters,TG and BL, on the outage performance. The figure provides two cases. In case1, we set $BL = 2.4$ and $TG = 0.05$ and in case2 we use $BL = 4.7$ and $TG = 0.1$. The figure indicates that the increase in the BL and TG causes a noticeable degradation in the OPs. This result is due to the increase in water turbulence with the increase in water BL and TG, which in turn degrades the performance.

The effect of the number of RIS reflecting elements N on the outage performance is illustrated in Fig. 4. It is clear that the increase in N has a remarkable enhancing effect on the values of OPs at low SNR, while this effect diminishes with the increase in transmission SNR. The explanation for this trend is that the increase in N leads to an increase in γ_R^1 and γ_R^2 according to (2) and (3) at low SNR. At high SNR the values of γ_R^1 and γ_R^2 saturates and the effect of N is negligible.

Figure 5 depicts the effect of the imperfect SIC residual power

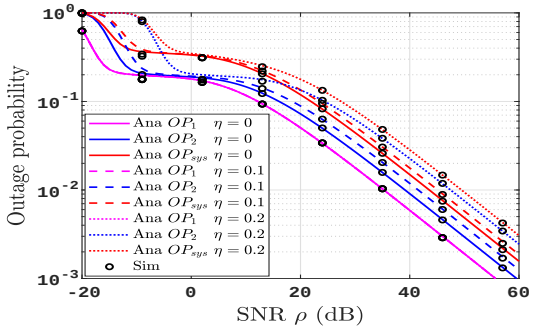

Figure 5. Effect of the imperfect SIC residual power (η) on OPs performance.

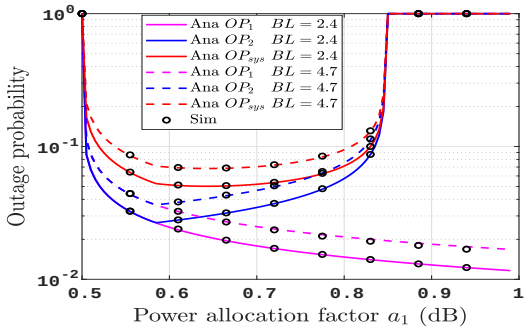

Figure 6. OPs over the entire range of power allocation factor at $\rho = 30$dB.

factor η on OPs performance of the proposed system by assuming three levels of $\eta = 0, 0.1, 0.2$. From the figure, we can notice that the higher value of η causes a higher degradation in OPs performance. The best performance is achieved with the perfect SIC scenario ($\eta = 0$), This is due to the fact that an increase in η leads to a higher interference level.

The effect of NOMA power allocation factor a_1 is discussed in Fig. 6, where a_1 varies over its entire range at $\rho = 30$dB. As expected, when the value of a_1 increases the value of γ_R^1 and $\gamma_{D_1}^1$ improves, consequently OP_1 witnesses a great improvement. Also, the figure shows two different trends of performance of OP_2 and $\mathrm{OP}_{\mathrm{sys}}$, the first is an improvement in the outage performance when the value of the a_1 is increased in its small range as D_2 needs to decode s_1 firstly before decoding its own message s_2. And when a certain value of a_1 is exceeded, the outage performance deteriorates since increasing a_1 means decreasing the a_2 that degrades the OP_2 and $\mathrm{OP}_{\mathrm{sys}}$. In the end, we notice an enhanced outage performance with the lower value of BL.

At the end of this discussion, in Fig. 7, we held a fair comparison between our proposed NOMA-based system and the same system topology that utilizes the OMA as a multiplexing technique. The result of this comparison indicates the superiority of our proposed system with a significant difference in the outage performance. This can be explained by referring to the main objective of using the NOMA technique to enhance spectral efficiency.

V. CONCLUSIONS

In this work, we investigated the outage performance of the NOMA-based RIS-assisted hybrid RF-UWOC system. We derived exact closed-form expressions for the outage probability in terms of Meijer's G-function and lower incomplete Gamma function and a tight asymptotic outage probability. The outage diversity order was obtained and it was found that it directly depends on the detection technology implemented in the UOWC destinations. We examined the outage performance dependency on many of the system parameters including the water turbulence, NOMA power allocation, receiver

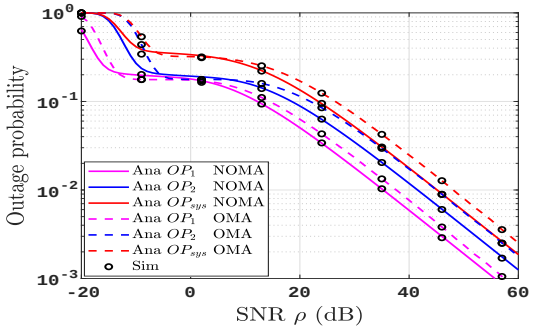

Figure 7. OPs performance under NOMA and OMA based system.

detection technique, and the imperfect SIC residual power factor. The results indicated the positive push made by raising the number of RIS elements. Also, As N increases, the UOWC link dominates the performance of the system. Besides, we illustrated the rule on NOMA in enhancing the performance via the comparison held against the benchmark OMA-based system.

ACKNOWLEDGMENT

This work was supported by Luxembourg National Research Fund (FNR) under the CORE project RISOTTI C20/IS/14773976.

REFERENCES

[1] X. Yuan, Y.-J. A. Zhang, Y. Shi, W. Yan, and H. Liu, "Reconfigurable-intelligent-surface empowered wireless communications: Challenges and opportunities," *IEEE Wireless Communications*, vol. 28, no. 2, pp. 136–143, 2021.

[2] G. C. Alexandropoulos, I. Vinieratou, and H. Wymeersch, "Localization via multiple reconfigurable intelligent surfaces equipped with single receive RF chains," *IEEE Wireless Communications Letters*, pp. 1–1, 2022.

[3] B. Di, H. Zhang, L. Li, L. Song, Y. Li, and Z. Han, "Practical hybrid beamforming with finite-resolution phase shifters for reconfigurable intelligent surface based multi-user communications," *IEEE Transactions on Vehicular Technology*, vol. 69, no. 4, pp. 4565–4570, 2020.

[4] Y. Pan, K. Wang, C. Pan, H. Zhu, and J. Wang, "Self-sustainable reconfigurable intelligent surface aided simultaneous terahertz information and power transfer (STIPT)," *IEEE Transactions on Wireless Communications*, pp. 1–1, 2022.

[5] X. Li, Z. Xie, Z. Chu, V. G. Menon, S. Mumtaz, and J. Zhang, "Exploiting benefits of IRS in wireless powered NOMA networks," *IEEE Transactions on Green Communications and Networking*, vol. 6, no. 1, pp. 175–186, 2022.

[6] J. Ye, S. Guo, S. Dang, B. Shihada, and M.-S. Alouini, "On the capacity of reconfigurable intelligent surface assisted MIMO symbiotic communications," *IEEE Transactions on Wireless Communications*, pp. 1–1, 2021.

[7] A.-A. A. Boulogeorgos and A. Alexiou, "Performance analysis of reconfigurable intelligent surface-assisted wireless systems and comparison with relaying," *IEEE Access*, vol. 8, pp. 94 463–94 483, 2020.

[8] A. Hemanth, K. Umamaheswari, A. C. Pogaku, D.-T. Do, and B. M. Lee, "Outage performance analysis of reconfigurable intelligent surfaces-aided NOMA under presence of hardware impairment," *IEEE Access*, vol. 8, pp. 212 156–212 165, 2020.

[9] J. Liu, J. Zhang, Q. Zhang, J. Wang, and X. Sun, "Secrecy rate analysis for reconfigurable intelligent surface-assisted mimo communications with statistical CSI," *China Communications*, vol. 18, no. 3, pp. 52–62, 2021.

[10] Y. Ai, F. A. P. deFigueiredo, L. Kong, M. Cheffena, S. Chatzinotas, and B. Ottersten, "Secure vehicular communications through reconfigurable intelligent surfaces," *IEEE Transactions on Vehicular Technology*, vol. 70, no. 7, pp. 7272–7276, 2021.

[11] X. Li, Q. Wang, M. Liu, J. Li, H. Peng, M. J. Piran, and L. Li, "Cooperative wireless-powered noma relaying for b5g iot networks with hardware impairments and channel estimation errors," *IEEE Internet of Things Journal*, vol. 8, no. 7, pp. 5453–5467, 2021.

[12] W. U. Khan, X. Li, M. Zeng, and O. A. Dobre, "Backscatter-enabled noma for future 6g systems: A new optimization framework under imperfect sic," *IEEE Communications Letters*, vol. 25, no. 5, pp. 1669–1672, 2021.

[13] W. U. Khan, M. A. Javed, T. N. Nguyen, S. Khan, and B. M. Elhalawany, "Energy-efficient resource allocation for 6g backscatter-enabled noma iov networks," *IEEE Transactions on Intelligent Transportation Systems*, pp. 1–11, 2021.

[14] A. Samir, M. Elsayed, A. A. El-Banna, K. Wu, and B. M. Elhalawany, "Performance of noma-based dual-hop hybrid powerline-wireless communication systems," *IEEE Transactions on Vehicular Technology*, pp. 1–1, 2022.

[15] B. M. ElHalawany, F. Jameel, D. B. da Costa, U. S. Dias, and K. Wu, "Performance analysis of downlink noma systems over κ-μ shadowed fading channels," *IEEE Transactions on Vehicular Technology*, vol. 69, no. 1, pp. 1046–1050, 2020.

[16] W. U. Khan, X. Li, A. Ihsan, M. A. Khan, V. G. Menon, and M. Ahmed, "Noma-enabled optimization framework for next-generation small-cell iov networks under imperfect sic decoding," *IEEE Transactions on Intelligent Transportation Systems*, pp. 1–10, 2021.

[17] W. U. Khan, X. Li, A. Ihsan, Z. Ali, and B. M. Elhalawany, "Energy efficiency maximization for beyond 5g NOMA-enabled heterogeneous networks," *Peer-to-Peer Netw. Appl.*, vol. 14, p. 3250–3264, 2021.

[18] W. U. Khan, F. Jameel, T. Ristaniemi, B. M. Elhalawany, and J. Liu, "Efficient power allocation for multi-cell uplink noma network," in *2019 IEEE 89th Vehicular Technology Conference (VTC2019-Spring)*, 2019, pp. 1–5.

[19] A. A. Aziz El-Banna, K. Wu, and B. M. ElHalawany, "Application of neural networks for dynamic modeling of an environmental-aware underwater acoustic positioning system using seawater physical properties," *IEEE Geoscience and Remote Sensing Letters*, vol. 19, pp. 1–5, 2022.

[20] A. A. Aziz El-Banna, A. B. Zaky, B. M. ElHalawany, J. Zhexue Huang, and K. Wu, "Machine learning based dynamic cooperative transmission framework for IoUT networks," in *2019 16th Annual IEEE International Conference on Sensing, Communication, and Networking (SECON)*, 2019, pp. 1–9.

[21] R. Ruby, S. Zhong, B. M. ElHalawany, H. Luo, and K. Wu, "SDN-enabled energy-aware routing in underwater multi-modal communication networks," *IEEE/ACM Transactions on Networking*, vol. 29, no. 3, pp. 965–978, 2021.

[22] B. M. ElHalawany, M. Elsabrouty, O. Muta, A. Abdelrahman, and H. Furukawa, "Zero-forcing relay power allocation for tdbc-based bidirectional relay networks," in *2014 International Conference on Information Science, Electronics and Electrical Engineering*, vol. 2, 2014, pp. 872–876.

[23] ——, "Joint energy-efficient single relay selection and power allocation for analog network coding with three transmission phases," in *2014 IEEE 79th Vehicular Technology Conference (VTC Spring)*, 2014, pp. 1–7.

[24] S. Li, L. Yang, D. B. da Costa, J. Zhang, and M.-S. Alouini, "Performance analysis of mixed RF-UWOC dual-hop transmission systems," *IEEE Trans. Veh. Technol.*, vol. 69, no. 11, pp. 14 043–14 048, 2020.

[25] S. Li, L. Yang, D. B. da Costa, and S. Yu, "Performance analysis of UAV-based mixed RF-UWOC transmission systems," *IEEE Trans. Commun.*, vol. 69, no. 8, pp. 5559–5572, 2021.

[26] M. Ibrahim, A. S.Badrudduza, M. S. Hossen, M. K. Kundu, and I. S. Ansari, "Enhancing security of TAS/MRC based mixed RF-UOWC system with induced underwater turbulence effect," *ArXiv*, vol. abs/2105.09088, 2021.

[27] Y. Lou, R. Sun, J. Cheng, D. Nie, and G. Qiao, "Secrecy outage analysis of two-hop decode-and-forward mixed RF/UWOC systems," *IEEE Commun. Lett.*, pp. 1–1, 2021.

[28] S. Li, L. Yang, D. B. d. Costa, M. D. Renzo, and M.-S. Alouini, "On the performance of ris-assisted dual-hop mixed rf-uwoc systems," *IEEE Transactions on Cognitive Communications and Networking*, vol. 7, no. 2, pp. 340–353, 2021.

[29] A. A. Aziz El-Banna and K. Wu, "Machine learning modeling for IoUT networks: Internet of underwater things," *Springer International Publishing*, 2021.

[30] E. Zedini, H. M. Oubei, A. Kammoun, M. Hamdi, B. S. Ooi, and M.-S. Alouini, "Unified statistical channel model for turbulence-induced fading in underwater wireless optical communication systems," *IEEE Trans. Commun.*, vol. 67, no. 4, pp. 2893–2907, 2019.

[31] V. S. Adamchik and O. I. Marichev, "The algorithm for calculating integrals of hypergeometric type functions and its realization in REDUCE system," *Association for Computing Machinery*, 1990.

[32] A.-A. A. Boulogeorgos and A. Alexiou, "Performance analysis of reconfigurable intelligent surface-assisted wireless systems and comparison with relaying," *IEEE Access*, vol. 8, pp. 94 463–94 483, 2020.

[33] I. Gradshteyn and I. Ryzhik, "Table of integrals, series, and products , eighth edition,," 2014.

[34] M. Elsayed, A. Samir, A. A. El-Banna, X. Li, and B. M. Elhalawany, "When NOMA multiplexing meets symbiotic ambient backscatter communication: Outage analysis," *IEEE Trans. Veh. Technol.*, pp. 1–1, 2021.